J. Phys. Earth, **41**, 87–101, 1993

Crustal Deformation Associated with Two-Dimensional Thrust Faulting

Sarva Jit Singh* and Sunita Rani

Department of Mathematics, Maharshi Dayanand University,
Rohtak-124001, India

The effect of the source-depth and the dip of the fault on the surface displacement field due to a long thrust fault embedded in an elastic half-space is studied. It is found that, for small dip angles, the displacement field is highly asymmetric about the fault strike, the displacement of the footwall is very small, and the horizontal displacement of the hanging wall shows a wavy pattern. The vertical displacement of the hanging wall is an uplift near the fault. For small dip angles, this uplift is maximum at a point almost vertically above the upper edge of the fault. As we go away from the fault strike, the vertical displacement changes sign, i.e., it becomes subsidence. For small dip angles, this subsidence is maximum at a point roughly vertically above the lower edge of the fault. Steeper fault dips decrease the subsidence relative to the uplift. For a vertical dip-slip fault, the horizontal displacement is completely symmetric about the fault strike and the vertical displacement is completely antisymmetric.

The variation of the coseismic and postseismic shear stresses and shear strains for a surface-breaking long thrust fault with depth is studied for a viscoelastic half-space. It is found that, while the coseismic and postseismic shear stresses are of opposite signs, the coseismic and postseismic shear strains are of the same sign.

1. Introduction

Two-dimensional dip-slip dislocation models have been used extensively to model the crustal deformations associated with thrust faulting at subduction zones (see, e.g., Cohen (1992) and the references listed therein). Savage *et al.* (1992) modelled the strain accumulation across the Wasatch fault near Ogden, Utah (U.S.A.) by a two-dimensional listric fault. Rani and Singh (1992) obtained closed-form analytical expressions for the displacements and stresses at any point of a homogeneous, isotropic, perfectly elastic half-space caused by a long dip-slip fault of finite width. Singh and Rani (1993) obtained the corresponding strains.

In order to study the effect of the source-depth and the dip of the fault, we compute the surface displacements caused by a long dip-slip fault of finite width placed in a homogeneous, isotropic, perfectly elastic half-space. Seven values of the dip angle,

Received March 1, 1993; Accepted June 24, 1993

* To whom correspondence should be addressed.

namely, $\delta=5°$, 15°, 30°, 45°, 60°, 75°, and 90°, are considered. For each δ, the surface displacements are computed for four source locations: a surface-breaking fault and three buried faults. The correspondence principle of linear viscoelasticity is used to obtain the postseismic stresses and strains at any point of the half-space. The variation of the coseismic and postseismic shear stresses and strains with depth is also investigated.

2. Surface Displacements

Dislocation models of faulting are often used to explain the observed coseismic deformations. Taking the x_1-axis along the strike of the fault and the x_3-axis vertically downwards, the surface displacements due to a two-dimensional dip-slip fault of finite width embedded in a uniform half-space ($x_3>0$) are given by(Rani and Singh (1992))

$$u_1=0\,, \tag{1}$$

$$u_2=\frac{b}{\pi}\left[\cos\delta\tan^{-1}\left(\frac{x_2-s\cos\delta}{s\sin\delta}\right)+\sin\delta(s-x_2\cos\delta)\frac{s}{R_0^2}\right]\Bigg|_{s_1}^{s_2}, \tag{2}$$

$$u_3=\frac{b}{\pi}\left[\sin\delta\tan^{-1}\left(\frac{x_2-s\cos\delta}{s\sin\delta}\right)+x_2\sin^2\delta\frac{s}{R_0^2}\right]\Bigg|_{s_1}^{s_2}, \tag{3}$$

where b is the magnitude of dislocation (slip), δ is the dip angle (Fig. 1) and

$$R_0^2=(x_2-s\cos\delta)^2+s^2\sin^2\delta\,. \tag{4}$$

We wish to examine the effect of the dip angle and the depth of the fault on the surface deformation due to a long thrust fault of finite width $L=s_2-s_1$ and infinite length embedded in a uniform half-space. For this purpose, we consider four different

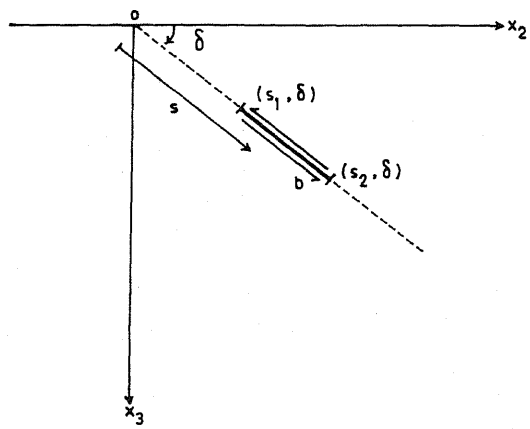

Fig. 1. Geometry of a long dip-slip fault. The displacement discontinuity b is perpendicular to the x_1-axis, but lies in the fault plane. The Cartesian coordinates of a point on the fault are ($s\cos\delta$, $s\sin\delta$), where δ is the dip angle and $s_1\leq s\leq s_2$.

positions of the fault:

$$\text{Source I} : \quad s_1 = 0, \quad s_2 = L$$
$$\text{Source II} : \quad s_1 = L, \quad s_2 = 2L$$
$$\text{Source III}: \quad s_1 = 2L, \quad s_2 = 3L$$

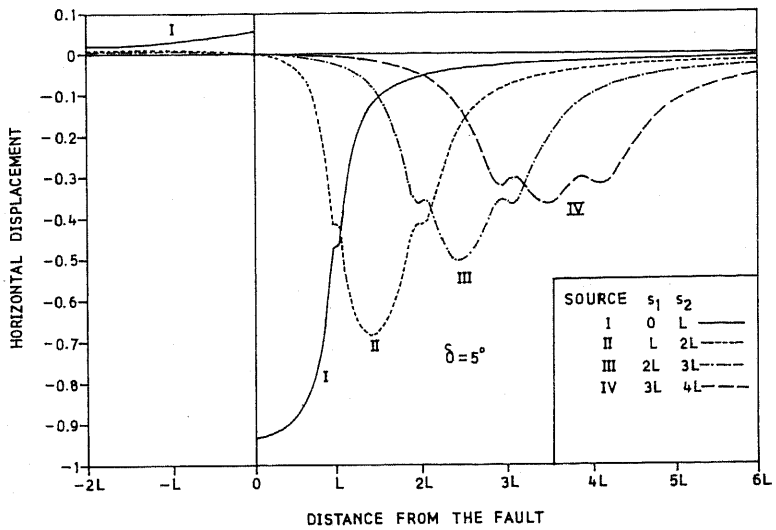

Fig. 2(a). Variation of the dimensionless horizontal displacement (u_2/b) with the distance from the fault (x_2) for dip angle $\delta = 5°$.

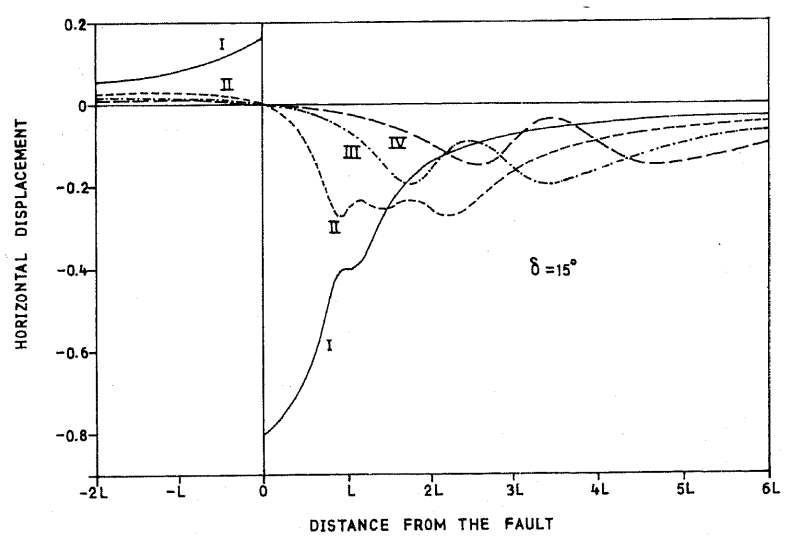

Fig. 2(b). Variation of the dimensionless horizontal displacement with x_2 for $\delta = 15°$.

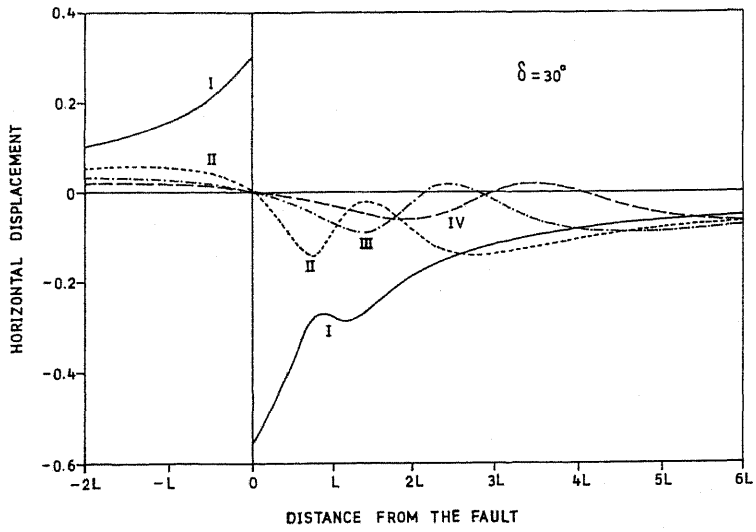

Fig. 2(c). Variation of the dimensionless horizontal displacement with x_2 for $\delta=30°$.

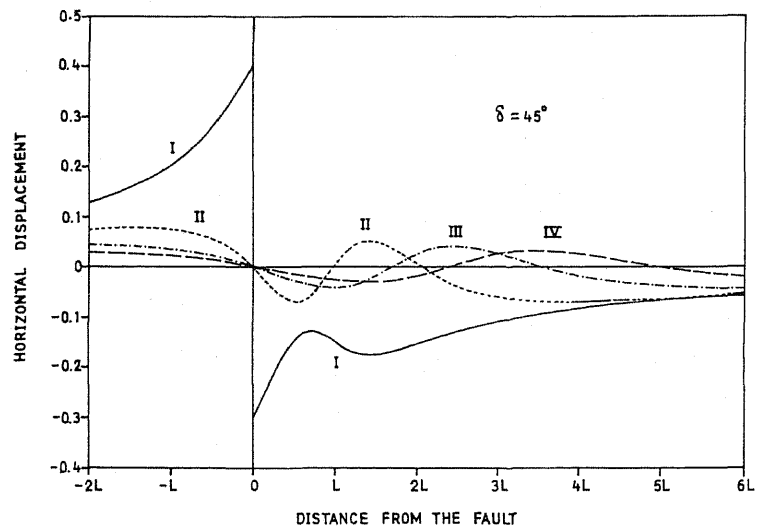

Fig. 2(d). Variation of the dimensionless horizontal displacement with x_2 for $\delta=45°$.

Source IV: $s_1=3L$, $s_2=4L$.

Figure 2(a) shows the variation of the dimensionless horizontal displacement (u_2/b) with the distance from the fault strike (x_2) for $\delta=5°$. We notice that the displacement field for the surface-breaking fault (Source I) is altogether different from the field for

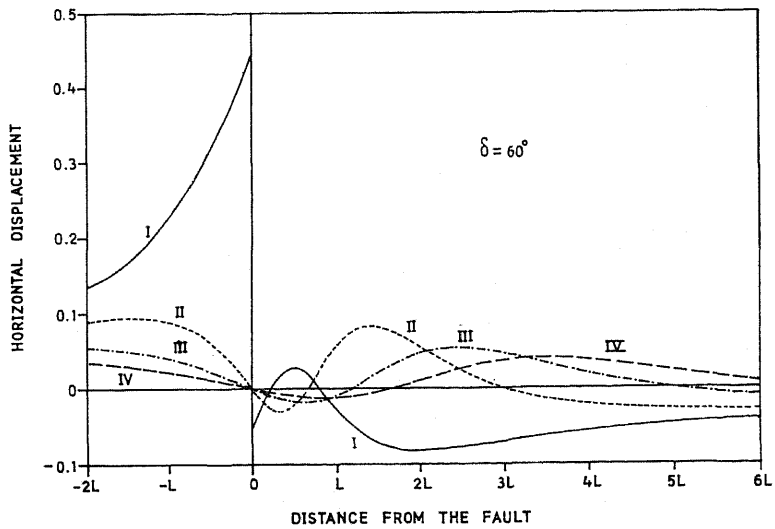

Fig. 2(e). Variation of the dimensionless horizontal displacement with x_2 for $\delta = 60°$.

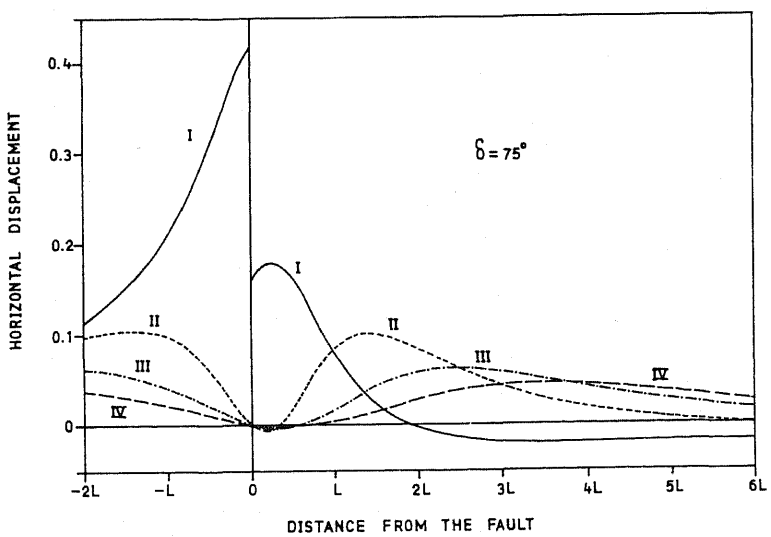

Fig. 2(f). Variation of the dimensionless horizontal displacement with x_2 for $\delta = 75°$.

the other three sources. For Source I, u_2 is discontinuous at $x_2 = 0$. For the other three sources, u_2 is continuous at $x_2 = 0$ and vanishes at that point. The variation of u_2 with x_2 for $\delta = 15°$ is shown in Fig. 2(b). Figure 2(c) is for $\delta = 30°$. For $x_2 > 0$, u_2 is negative for Sources I and II, but u_2 changes sign twice for Sources III and IV. Figure 2(d) is

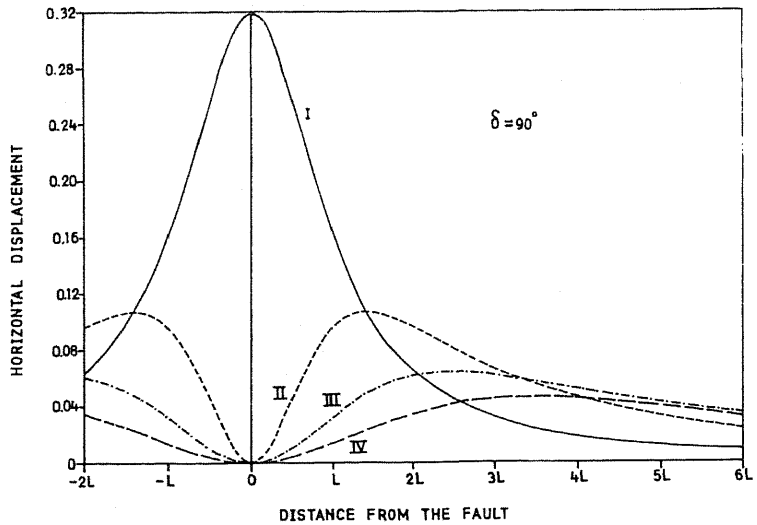

Fig. 2(g). Variation of the dimensionless horizontal displacement with x_2 for $\delta=90°$. The horizontal displacement is symmetric about the origin.

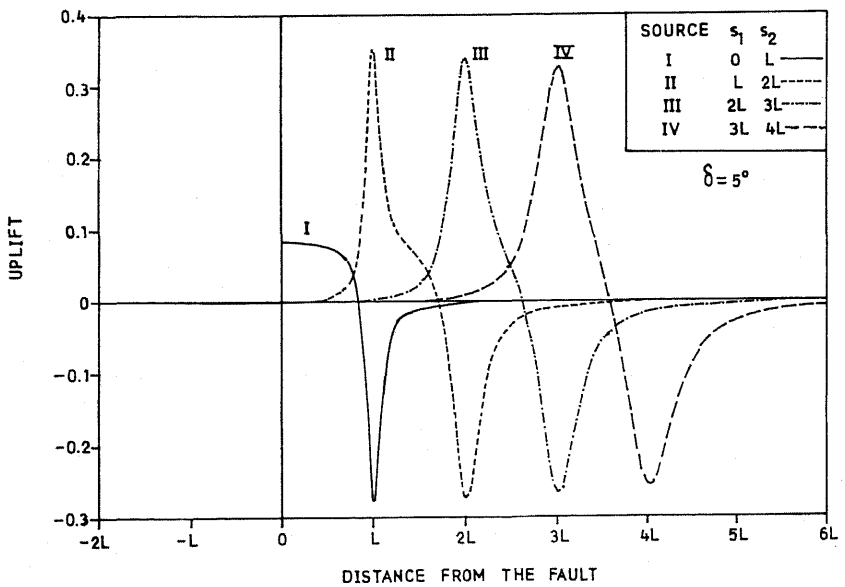

Fig. 3(a). Variation of the uplift ($-u_3$) with the distance from the fault (x_2) for $\delta=5°$. The uplift is measured in units of the slip b.

for $\delta=45°$. In this case, for $x_2>0$, u_2 is negative for Source I, but u_2 changes sign twice for Sources II, III, and IV. For $\delta=60°$, (Fig. 2(e)), u_2 changes sign twice for $x_2>0$ even for Source I. For $\delta=75°$, (Fig. 2(f)), even though u_2 is positive for Source I near

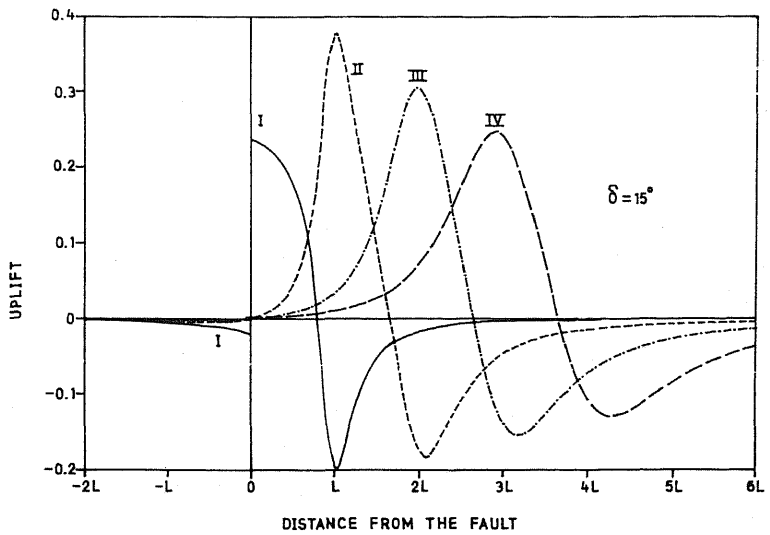

Fig. 3(b). Variation of the uplift with x_2 for $\delta=15°$.

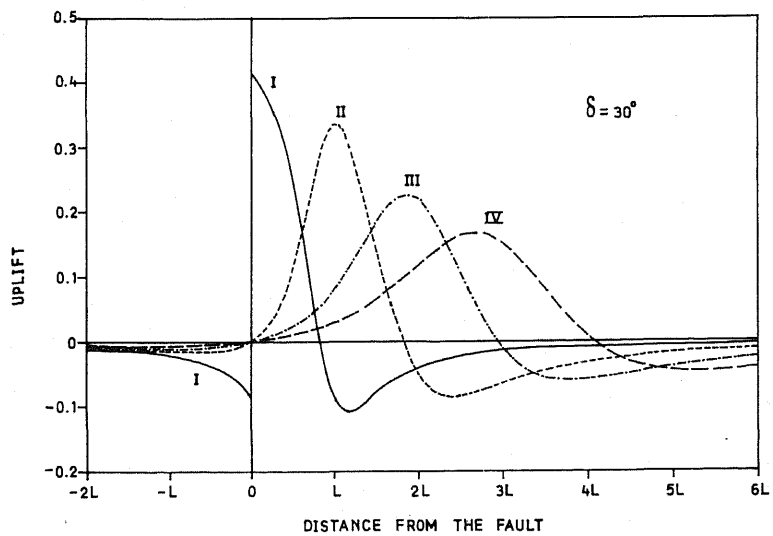

Fig. 3(c). Variation of the uplift with x_2 for $\delta=30°$.

the origin for both $x_2>0$ and $x_2<0$, it is discontinuous at the origin. As shown in Fig. 2(g), u_2 is completely symmetric about the origin for a vertical dip-slip fault.

The degree of asymmetry of the horizontal displacement u_2 about the origin and the discontinuity of u_2 for the surface-breaking thrust fault at the origin is controlled by the dip angle δ. The horizontal displacement is highly asymmetric for small values of δ. The discontinuity of u_2 at the origin is equal to $b\cos\delta$. These observations can

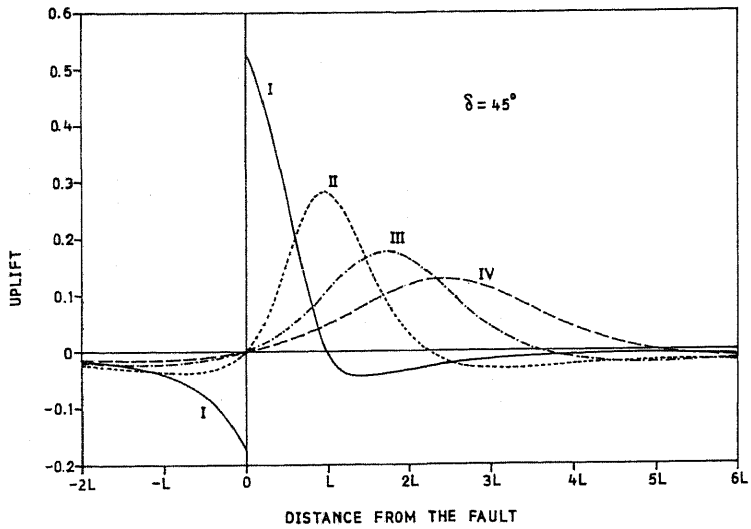

Fig. 3(d). Variation of the uplift with x_2 for $\delta=45°$.

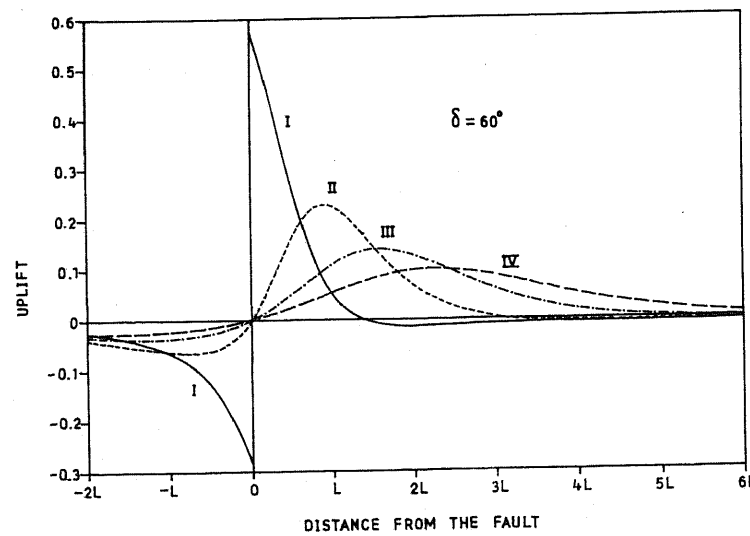

Fig. 3(e). Variation of the uplift with x_2 for $\delta=60°$.

be used in modelling surface deformation data.

Figure 3(a) shows the variation of the uplift ($-u_3$) in units of the slip b with the distance from the fault strike (x_2) for $\delta=5°$. We notice that the uplift is almost zero for $x_2<0$. u_3 is discontinuous at the origin for Source I, but vanishes there for Sources II, III, and IV. Moreover, u_3 vanishes once for $x_2>0$. Figure 3(b), 3(c), 3(d), 3(e), and 3(f) are for $\delta=15°$, 30°, 45°, 60°, and 75°, respectively. For $\delta=90°$ (Fig. 3(g)), u_3 is

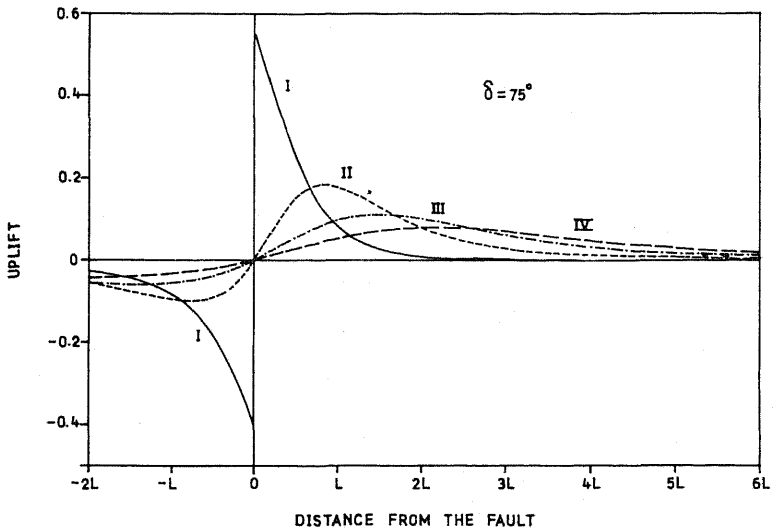

Fig. 3(f). Variation of the uplift with x_2 for $\delta=75°$.

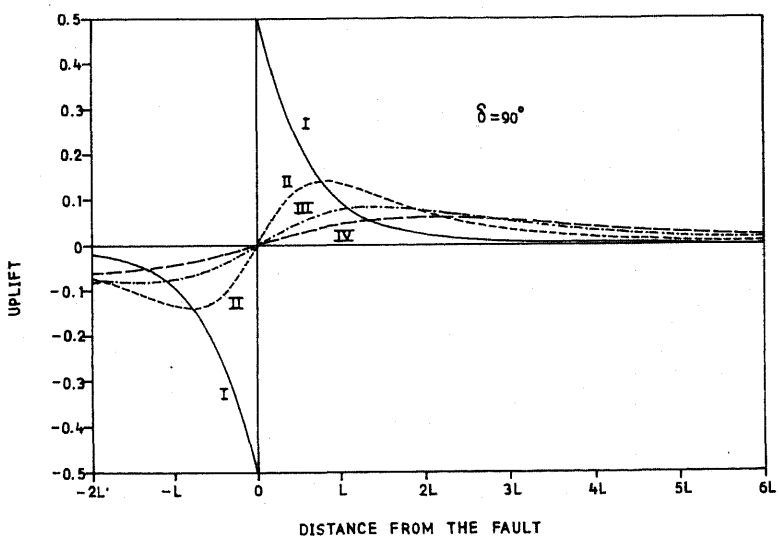

Fig. 3(g). Variation of the uplift with x_2 for $\delta=90°$. The uplift is antisymmetric about the origin.

antisymmetric about the origin. It is discontinuous at the origin for Source I, but vanishes there for Sources II, III, and IV.

As in the case of the horizontal displacement, the degree of asymmetry of the vertical displacement u_3 about the origin and the discontinuity of u_3 for the surface-breaking fault at the origin are controlled by the dip angle δ. For Source I, the discontinuity of

Table 1. Values of x_2/L for which the uplift of the hanging wall is maximum, the uplift vanishes and the subsidence is maximum for the four sources for different values of the dip angle δ. The values of the maximum uplift/subsidence of the hanging wall are also given.

Source	I $s_1=0,\ s_2=L$							II $s_1=L,\ s_2=2L$							III $s_1=2L,\ s_2=3L$							IV $s_1=3L,\ s_2=4L$						
Dip angle	5°	15°	30°	45°	60°	75°	90°	5°	15°	30°	45°	60°	75°	90°	5°	15°	30°	45°	60°	75°	90°	5°	15°	30°	45°	60°	75°	90°
Maximum uplift																												
x_2/L	0	0	0	0	0	0	0	1.00	1.02	1.00	0.94	0.89	0.84	0.80	2.01	1.98	1.84	1.70	1.57	1.48	1.40	3.00	2.90	2.65	2.42	2.25	2.10	2.00
Value	0.09	0.24	0.42	0.53	0.58	0.56	0.50	0.35	0.38	0.34	0.28	0.23	0.18	0.14	0.34	0.30	0.23	0.18	0.14	0.11	0.08	0.33	0.25	0.17	0.13	0.10	0.08	0.06
Zero uplift																												
x_2/L	0.85	0.79	0.82	0.97	1.35	2.58	—	1.71	1.65	1.80	2.20	3.11	*	—	2.61	2.63	2.92	3.58	5.06	*	—	3.57	3.65	4.07	4.98	*	*	—
Maximum subsidence																												
x_2/L	1.00	1.04	1.15	1.41	2.00	3.75	—	2.01	2.08	2.40	3.07	4.50	*	—	3.01	3.17	3.79	4.90	*	*	—	4.02	4.30	5.20	*	*	*	—
Value	0.28	0.20	0.11	0.05	0.02	0.00	—	0.27	0.18	0.08	0.03	0.01	*	—	0.27	0.16	0.06	0.02	*	*	—	0.26	0.13	0.05	*	*	*	—

* No value in the range $0<x_2<6L$.

u_3 at the origin is $b\sin\delta$. For small values of δ, the vertical displacement of the footwall is very small; the uplift (or subsidence) occurring mainly on the hanging wall. Table 1 describes the behavior of u_3 for $x_2>0$ for the four sources. This table can be used in modelling observed uplift data.

3. Shear Strain

The shear strain e_{23} due to a two-dimensional dip-slip fault of finite width placed in a half-space ($x_3>0$) is given by (Rani and Singh (1992))

$$\begin{aligned} e_{23}=\frac{\alpha b}{2\pi}\Bigg\{&(x_2\cos\delta-x_3\sin\delta-s\cos2\delta)\left(\frac{1}{R^2}-\frac{1}{S^2}\right)\\ &+2(x_2\sin\delta-x_3\cos\delta)(x_2-s\cos\delta)\left[(x_3-s\sin\delta)\frac{1}{R^4}-(x_3+s\sin\delta)\frac{1}{S^4}\right]\\ &+4\sin\delta\left[x_3\sin\delta(x_3+s\sin\delta)+(x_2\sin\delta+2x_3\cos\delta)(x_2-s\cos\delta)\right]\frac{s}{S^4}\\ &-16x_3\sin\delta(x_2\sin\delta+x_3\cos\delta)(x_2-s\cos\delta)(x_3+s\sin\delta)\frac{s}{S^6}\Bigg\}\Bigg|_{s_1}^{s_2}, \end{aligned} \tag{5}$$

where

$$\alpha=\frac{\lambda+\mu}{\lambda+2\mu},$$

$$R^2=(x_2-s\cos\delta)^2+(x_3-s\sin\delta)^2, \tag{6}$$

$$S^2=(x_2-s\cos\delta)^2+(x_3+s\sin\delta)^2, \tag{7}$$

λ, μ being the Lamé constants.

The quasi-static strain for a viscoelastic half-space can be obtained from Eq. (5) on replacing $b\alpha$ by (Singh and Singh (1990))

$$b_0\left[1-(1-\alpha)\exp\left(-\frac{4\alpha-1}{3}\cdot\frac{t}{\tau}\right)\right]H(t), \tag{8}$$

where τ is the relaxation time. Equation (8) assumes that the medium is elastic in dilatation and Maxwell viscoelastic in distortion, and that the source has unit step function time-dependence:

$$b(t)=b_0H(t).$$

The coseismic shear strain is modelled by the static strain given by Eq. (5). The post-seismic strain is obtained on subtracting the static strain from the quasi-static strain obtained on using the correspondence (8).

Figure 4(a), 4(b), and 4(c) show the variation of the coseismic and postseismic shear strains with depth (x_3) for $x_2=L/2$, L and $2L$, respectively, for a surface-breaking fault (Source I) dipping at 30° in a Poissonian ($\lambda=\mu$) half-space. We notice that the

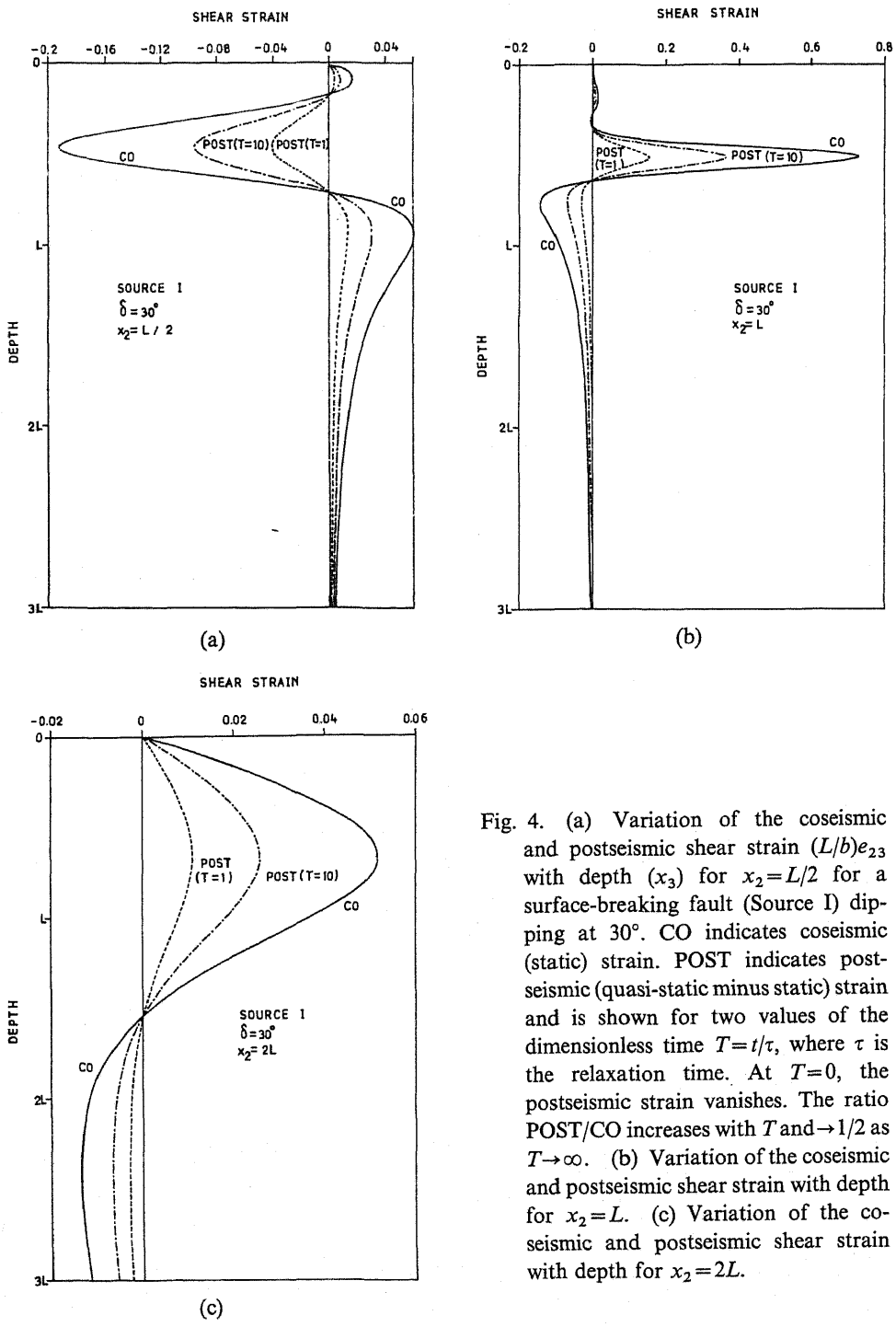

Fig. 4. (a) Variation of the coseismic and postseismic shear strain $(L/b)e_{23}$ with depth (x_3) for $x_2=L/2$ for a surface-breaking fault (Source I) dipping at 30°. CO indicates coseismic (static) strain. POST indicates postseismic (quasi-static minus static) strain and is shown for two values of the dimensionless time $T=t/\tau$, where τ is the relaxation time. At $T=0$, the postseismic strain vanishes. The ratio POST/CO increases with T and $\to 1/2$ as $T\to\infty$. (b) Variation of the coseismic and postseismic shear strain with depth for $x_2=L$. (c) Variation of the coseismic and postseismic shear strain with depth for $x_2=2L$.

coseismic and postseismic shear strains are of the same sign.

4. Shear Stress

The shear stress is obtained from Eq. (5) on using the relation

$$\tau_{23}=2\mu e_{23}\,.$$

The quasi-static stress for a viscoelastic half-space can then be obtained on replacing $b\mu\alpha$ by (Singh and Singh (1990))

$$\frac{1}{4}b_o\mu\left[\exp\left(-\frac{t}{\tau}\right)+(4\alpha-1)\exp\left(-\frac{4\alpha-1}{3}\cdot\frac{t}{\tau}\right)\right]H(t)\,.$$

Figure 5(a), 5(b), and 5(c) show the variation of the coseismic and postseismic shear stresses with depth for $x_2=L/2$, L, and $2L$, respectively, for a surface-breaking fault dipping at 30° in a Poissonian half-space. We notice that the coseismic and postseismic shear stresses are of opposite signs.

5. Discussion and Conclusions

For a surface-breaking long thrust fault (Source I), the horizontal displacement is discontinuous at the origin (upper edge of the fault), the magnitude of discontinuity being $b\cos\delta$, where b is the slip on the fault and δ is the dip angle. Similarly, the vertical displacement has a discontinuity of magnitude $b\sin\delta$ at the origin.

From Eq. (2) we find that, for Source I, the horizontal displacement (u_2) on the hanging wall side has a maximum at $x_2=L\cos\delta$ and a minimum at $x_2=L/\cos\delta$. Moreover,

$$(u_2)_{\max}=\frac{b}{\pi}(\sin\delta-\frac{\pi}{2}\cos\delta)\,,$$

$$(u_2)_{\min}=b\cos\delta(\delta/\pi-1/2)\,.$$

For small dip angles, the two stationary points are close to each other. This explains the short wavelength oscillations in the graphs for the horizontal displacement for Source I in Fig. 2(a), 2(b), and 2(c). A similar interpretation can be given to the short wavelength oscillations in the graphs for the horizontal displacement in respect of the other three sources. For example, in Fig. 2(a), the graph for Source II has two small wavelength oscillations, corresponding to the two edges of the fault. However, as the distance of the edges from the free surface increases, the stationary points separate out, and we get a wavy pattern (see, e.g., the graphs for Source II in Fig. 2(c), Source III in Fig. 2(b), and Source IV in Fig. 2(a)).

Equation (3) reveals that, for Source I, the subsidence (u_3) on the hanging wall side is maximum at the point $x_2=L/\cos\delta$ and

$$(u_3)_{\max}=\frac{b}{\pi}\left[\cos\delta-\left(\frac{\pi}{2}-\delta\right)\sin\delta\right].$$

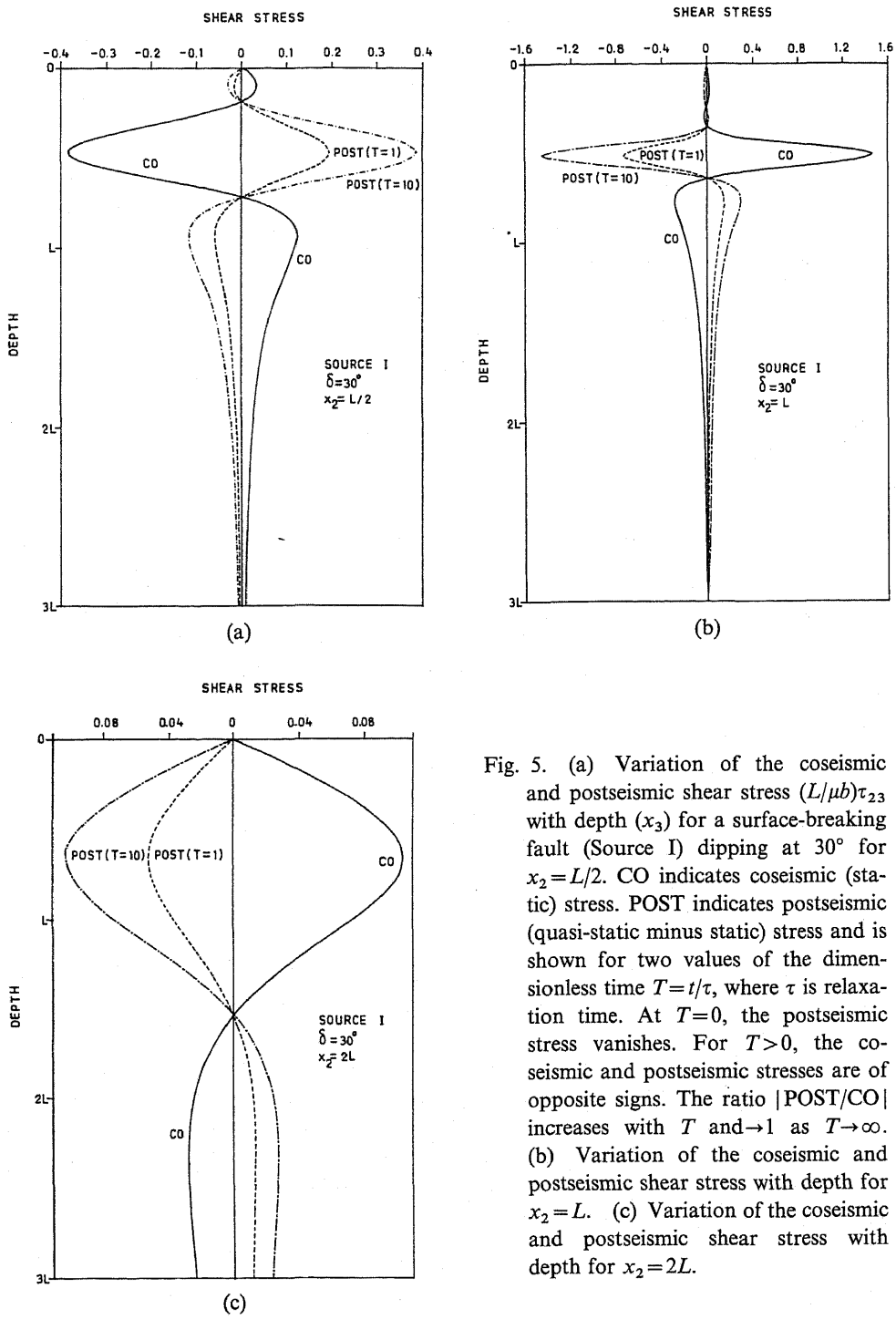

Fig. 5. (a) Variation of the coseismic and postseismic shear stress $(L/\mu b)\tau_{23}$ with depth (x_3) for a surface-breaking fault (Source I) dipping at 30° for $x_2=L/2$. CO indicates coseismic (static) stress. POST indicates postseismic (quasi-static minus static) stress and is shown for two values of the dimensionless time $T=t/\tau$, where τ is relaxation time. At $T=0$, the postseismic stress vanishes. For $T>0$, the coseismic and postseismic stresses are of opposite signs. The ratio |POST/CO| increases with T and$\rightarrow 1$ as $T\rightarrow\infty$. (b) Variation of the coseismic and postseismic shear stress with depth for $x_2=L$. (c) Variation of the coseismic and postseismic shear stress with depth for $x_2=2L$.

The maximum subsidence is a decreasing function of δ.

Table 1 gives the values of x_2/L for which the uplift of the hanging wall is maximum, the uplift vanishes and the subsidence is maximum. We note that, for small dip angles, the uplift for buried faults (Sources II, III, and IV) is maximum at a point almost vertically above the upper edge of the fault. As we go away from the fault strike, the vertical displacement changes. For small dip angles, this subsidence is maximum at a point roughly vertically above the lower edge of the fault ($x_2 = s_2/\cos\delta$ is a better approximation). The maximum uplift is greater than the maximum subsidence. Steeper fault dips decrease the subsidence relative to the uplift. The results of Table 1 should prove useful in modelling surface deformation data.

We are grateful to the University Grants Commission, New Delhi, for financial support. The comments of the two referees led to an improvement in the presentation of the paper and interpretation of results.

REFERENCES

Cohen, S. C., Postseismic deformation and stress diffusion due to viscoelasticity and comments on the modified Elasser model, *J. Geophys. Res.*, **97**, 15395–15403, 1992.

Rani, S. and S. J. Singh, Static deformation of a uniform half-space due to a long dip-slip fault, *Geophys. J. Int.*, **109**, 469–476, 1992.

Savage, J. C., M. Lisowski, and W. H. Prescott, Strain accumulation across the Wasatch Fault near Odgen, Utah, *J. Geophys. Res.*, **97**, 2071–2083, 1992.

Singh, K. and S. J. Singh, A simple procedure for obtaining the quasistatic displacements, strains and stresses in a viscoelastic half-space, *Bull. Seismol. Soc. Am.*, **80**, 488–492, 1990.

Singh, S. J. and S. Rani, Subsurface deformation due to long strike-slip and dip-slip faults in a uniform half-space, *Proc. Indian Acad. Sci. (Earth Planet. Sci.)*, 1993 (in press).